Nozzle Geometry Effects on Corner Boundary-Layers in Supersonic Wind Tunnels

Kshitij Sabnis* and Holger Babinsky[†]
Department of Engineering, University of Cambridge, Cambridge, CB2 1PZ, UK

I. Introduction

EXPERIMENTS on supersonic flows are typically conducted in wind tunnels with rectangular cross-sections, which use two-dimensional nozzles of two different types. A "full" setup consists of two contoured nozzle surfaces symmetric about the tunnel centre-height. The "half" configuration is also common, with a curved ceiling nozzle surface and a straight horizontal floor [1].

Many experiments in supersonic flow focus on shock-induced separation, where the response of the tunnel boundary-layers to an incident shock is investigated. It has been shown that the onset and shape of the separation on the floor are dependent on the size of corner separation [2–6]. This corner separation is strongly affected by the momentum within the corner boundary-layer (the intersection between the sidewall and floor boundary-layers). For cases with otherwise identical floor boundary-layers, there are two factors which determine the momentum in the corner: first, the sidewall boundary-layer thickness and second, the structure of streamwise vortices produced by the Reynolds stresses in this region [7].

Both full and half nozzle configurations are commonly used in such experiments and have generally been considered to be equivalent. However, there is some evidence that this assumption may not be entirely correct. Past studies, admittedly in different facilities and at different Mach numbers, have observed distinct corner flow topologies for different nozzle geometries [8–13]. This experimental study examines the influence of nozzle configuration on the tunnel sidewall and corner boundary-layers, by using both the full and half setups in the same facility.

II. Research Methodology

Experiments are performed in Supersonic Wind Tunnel No. 1 at Cambridge University Engineering Department. This is a blow-down wind tunnel, driven by a high-pressure reservoir. The nominal freestream Mach number is fixed at $M_\infty = 2.5$ for this study. The tunnel is operated in both a full and half nozzle configuration, as depicted in figure 1.

An empty wind tunnel configuration is used in this study, and the measurements focus on the turbulent, naturally-grown boundary-layers on the tunnel's floor and sidewalls. The rectangular working section of the tunnel has a width of 114 mm, and a height of 172 mm and 86 mm for the full and half configurations respectively. The coordinate system

---

*PhD Student, Department of Engineering, University of Cambridge.
[†]Professor in Aerodynamics, Department of Engineering, University of Cambridge, AIAA Associate Fellow.

convention is shown in figure 1: x represents the streamwise direction, as measured from the end of the nozzle; y indicates the floor-normal direction, with $y = 0$ mm set at the tunnel floor; z is the spanwise coordinate measured from the centre-span, such that $z = \pm 57$ mm correspond to the tunnel sidewalls. The stagnation pressure is set to 308 ± 1 kPa and the operating stagnation temperature is measured as 285 ± 5 K; this corresponds to a nominal unit Reynolds number of 31×10^6 m^{-1}. Within the optically accessible region of the working section (60–120 mm downstream of the nozzle exit), the tunnel boundary-layers are approximately 7 mm to 8 mm thick. They therefore have a Reynolds number based on incompressible displacement thickness of around $\mathrm{Re}_{\delta_i^*} = 30,000$.

The streamwise and vertical flow velocities, u and v respectively, are measured by two-component Laser Doppler Velocimetry (LDV). The flow is seeded with paraffin in the settling chamber; previous measurements of particle lag through a normal shock have placed the seeding droplet diameter in the range $200 - 500$ nm [14]. The measured velocities have an uncertainty of 1% and 14% for u and v respectively; there are error contributions from the rate of seeding particles and the laser optics. Traverses are carried out with spatial resolution of 0.1 mm inside the boundary-layers and 1 mm in the freestream. The ellipsoidal probe volume spans 0.1 mm in the streamwise direction and 2 mm in the spanwise direction. Regions with insufficient data quality (less than 1000 velocity measurements per data point) are excluded from the analysis.

III. Results and Discussion

A. Sidewall secondary flows

For both setups, the flowfield is surveyed 120mm downstream of the nozzle exit. Figure 2 presents the vertical velocities over the tunnel cross-section. Within the core flow, the vertical velocities do not exceed 1% of u, which is within experimental error. However, there is a significant vertical velocity component (5% of u) within the sidewall boundary-layers, indicative of a secondary flow. The vertical velocities are directed towards the tunnel centre-height in the full setup and in the downwards direction with the half configuration. These will be referred to as sidewall secondary flows.

The hypothesised mechanism for the sidewall secondary flows is related to the pressure distribution in the nozzle as depicted schematically in figure 3. We will first consider the full setup. The dashed line in figure 3a.i lies approximately half-way between the nozzle throat and exit. Here, the flow at the centre-height has expanded to the test section pressure while the pressure is higher at the top and bottom of the tunnel. Similar arguments hold elsewhere in the nozzle, since the pressure drop on the curved surface lags behind that at the centre-height. This sets up a vertical pressure gradient (figure 3a.ii). The sidewall boundary-layers, with low momentum flow, are most susceptible to this pressure gradient. A secondary vertical flow is therefore introduced in these sidewall boundary-layers from the channel corners to the tunnel centre-height (figure 3a.iii). The corresponding mechanism for the half configuration is presented in figure 3b.

There is no vertical pressure gradient in the working section itself, so the sidewall secondary flows are expected to dissipate with streamwise distance. However, the optically accessible region in this wind tunnel extends over only 60 mm in the streamwise direction – this corresponds to just 0.35 or 0.7 tunnel heights for the two setups. Within this region, there is no measurable dissipation of the secondary flow.

B. Effect on sidewall boundary-layers

The sidewall boundary-layer thickness is affected by the vertical secondary flows, which transport the low momentum fluid in these regions. Streamwise velocities across the tunnel cross-section are given in figure 4. The core flow is evident for both configurations, as are the tunnel boundary-layers. While the floor and ceiling boundary-layers have approximately constant thickness across the tunnel span, the sidewall boundary-layer thickness varies considerably. In the full setup, the sidewall boundary-layers increase in thickness from the corners towards the centre-height; with the half setup, they get thicker from the top to the bottom of the tunnel. These variations are consistent with the identified secondary flows for both configurations.

C. Effect on corner boundary-layers

The streamwise velocity for all four tunnel corners, measured 120 mm downstream of the nozzle exit, is shown for both setups (figure 5). There appear to be two distinct flow topologies. All four corners of the full setup and the top corners of the half configuration are similar in nature. Meanwhile, the bottom corners of the half setup, with a thicker sidewall boundary-layer, have a larger low momentum region in the corner itself.

A closer inspection of the flowfield identifies some regions where the high momentum core flow persists into the boundary-layer and others where low momentum fluid extends locally into the core. On the figure, these regions are indicated by dashed arrows which show the approximate location and direction of these momentum transfers. It is thought that these are caused by streamwise vortices embedded in the viscous corner flow regions. The momentum transfers in the bottom corners of the half setup would be consistent with the presence of two counter-rotating vortices, while the other measured corners would appear to contain only a single primary vortex residing on the floor or ceiling.

These different inferred vortex structures can be understood in the context of the sidewall secondary flows. In a supersonic channel with turbulent wall boundary-layers but no vertical velocities, Gessner has proposed that the Reynolds stresses in the corner boundary-layer generate two counter-rotating streamwise-aligned vortices, symmetric about the corner bisector [7, 8]. The topology of these two vortices, referred to as the sidewall vortex and the floor vortex (figure 6a), are modified by the sidewall secondary flows. The floor vortex, residing outside the sidewall boundary-layer, is largely unaffected by any vertical flow. However, the sidewall vortex is influenced by the local vertical velocities; the secondary flows cause advection of any pre-existing sidewall vortex, as well as the continuously-produced 'sidewall vorticity'.

The case with vertical velocity directed away from the corners, (the full setup and the top corners of the half setup) is shown schematically in figure 6b. Any vorticity near the tunnel sidewall is immediately advected away from the corner by the vertical flow. This prevents the formation of a stable sidewall vortex, and so the corner region contains just one (floor) vortex. There is some evidence for this mechanism in recent experiments by Peltier *et al.* [13], performed in a supersonic channel flow with a "full" nozzle: the instantaneous flowfields capture a vortex pair, but there is only a single floor vortex present in the ensemble-averaged flow.

Figure 6c presents the opposite case, when the sidewall secondary flow is directed into the corner (the bottom corners of the half setup). Now, the sidewall vortex is advected towards the corner by the bulk vertical velocity. Therefore, the region retains the counter-rotating vortex pair.

IV. Conclusions

In conclusion, this study has identified the presence of sidewall secondary flows, which take distinct forms for the two nozzle geometries tested. The mechanism for the generation of these flows is based on the pressure distribution in the nozzle. These vertical velocities within the sidewall boundary-layers are responsible for modifying the sidewall boundary-layer thickness and the topology of the corner vortices. The corner flowfields are therefore quite different between the full and half nozzle configurations.

The separation properties of the corner boundary-layer under an adverse pressure gradient are dependent on the momentum in the corner region. This is influenced both by the thickness of the sidewall boundary-layer and by the properties of the vortices which entrain high-momentum core flow into the corner. Both these factors are intimately associated with the sidewall secondary flows. While their relative importance is yet to be established, the larger corner boundary-layers on the flat side of the half setup suggest that these corners are likely to exhibit earlier separation than either the contoured surface or the full setup.

The prevalence of two-dimensional nozzles within supersonic wind tunnel setups means that sidewall secondary flows are almost ubiquitous. They apparently have a significant influence on the sidewall and corner boundary-layers. Therefore, experimental studies on these regions or on shock-induced floor boundary-layer separation should consider the effects of these transverse velocities. Furthermore, when validating numerical codes using experimental data, the corner flowfield itself cannot be accurately computed without a knowledge of the nozzle geometry, and thus the sidewall secondary flows.

References

[1] Ferri, A., *Elements of aerodynamics of supersonic flows*, Macmillan Company, 1949.

[2] Chriss, R., Hingst, W., Strazisar, A., and Keith, T., "An LDA investigation of three-dimensional normal shock wave boundary-layer interactions," *Proceedings of Transonic Symposium: Theory, Application and Experiment*, Vol. 1 (Part 2), 1989, pp. 741–764.

[3] Bruce, P., Babinsky, H., Tartinville, B., and Hirsch, C., "Corner effect and asymmetry in transonic channel flows," *AIAA Journal*, Vol. 49, No. 11, 2011, pp. 2382–2392. doi:10.2514/1.j050497.

[4] Benek, J., Suchyta, C., and Babinsky, H., "The effect of tunnel size on incident shock boundary layer interaction experiments," *51st AIAA Aerospace Sciences Meeting including the New Horizons Forum and Aerospace Exposition*, 2013-0862. doi:10.2514/6.2013-862.

[5] Xiang, X., and Babinsky, H., "Corner effects in oblique shock wave/boundary layer interactions in rectangular channels," *55th AIAA Aerospace Sciences Meeting*, 2017-0984. doi:10.2514/6.2017-0984.

[6] Xiang, X., and Babinsky, H., "An experimental study of corner flow control applied to an oblique shock-wave/boundary-layer interaction," *56th AIAA Aerospace Sciences Meeting*, 2018-1532. doi:10.2514/6.2018-1532.

[7] Gessner, F., "The origin of secondary flow in turbulent flow along a corner," *Journal of Fluid Mechanics*, Vol. 58, No. 1, 1973, pp. 1–25. doi:10.1017/s0022112073002090.

[8] Gessner, F., Ferguson, S., and Lo, C., "Experiments on supersonic turbulent flow development in a square duct," *AIAA Journal*, Vol. 25, No. 5, 1987, pp. 690–697. doi:10.2514/3.9684.

[9] Davis, D., and Gessner, F., "Further experiments on supersonic turbulent flow development in a square duct," *AIAA Journal*, Vol. 27, No. 8, 1989, pp. 1023–1030. doi:10.2514/3.10216.

[10] Davis, D., Gessner, F., and Kerlick, G., "Experimental and numerical investigation of supersonic turbulent flow through a square duct," *AIAA Journal*, Vol. 24, No. 9, 1986, pp. 1508–1515. doi:10.2514/3.9473.

[11] Morajkar, R., Driscoll, J., and Gamba, M., "Experimental study of supersonic turbulent corner flow evolution in a low aspect ratio rectangular channel," *53rd AIAA Aerospace Sciences Meeting*, 2015-0542. doi:10.2514/6.2015-0542.

[12] Rice, B., Bisek, N., Peltier, S., and Hofferth, J., "Investigation of secondary motion in high speed flow," *55th AIAA Aerospace Sciences Meeting*, 2017-0526. doi:10.2514/6.2017-0526.

[13] Peltier, S., Rice, B., Bisek, N., McKenna, C., and Hofferth, J., "Structure of secondary motion in a Mach 2 boundary layer," *2018 AIAA Aerospace Sciences Meeting*, 2018-0583. doi:10.2514/6.2018-0583.

[14] Colliss, S., Babinsky, H., Nübler, K., and Lutz, T., "Vortical structures on three-dimensional shock control bumps," *AIAA Journal*, 2016, pp. 2338–2350. doi:10.2514/1.j054669.
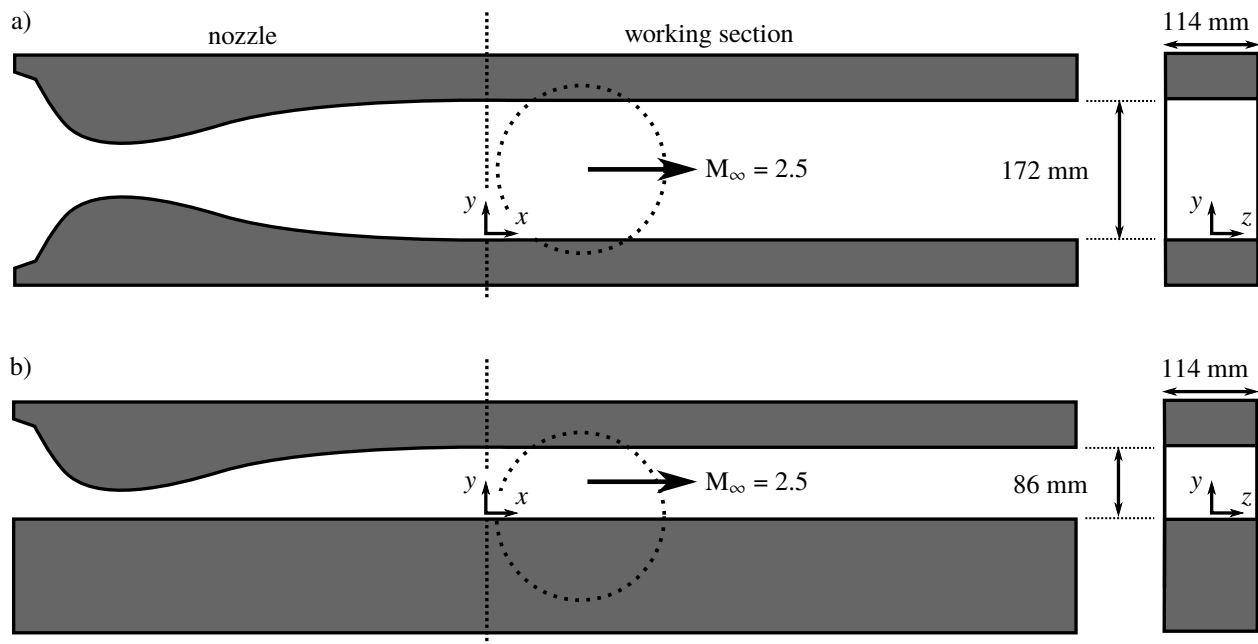
Fig. 1 **Tunnel setup for a) the full and b) the half configurations. The dashed circle corresponds to a window in the tunnel wall providing optical access.**
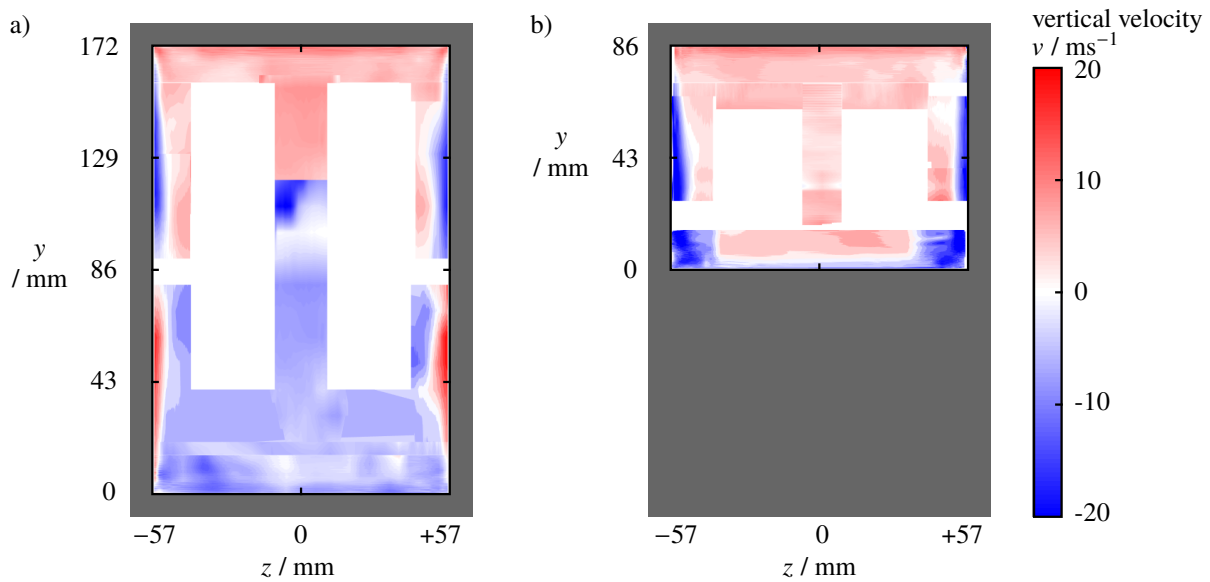

Fig. 2 **Distribution of vertical velocity (v) across the tunnel cross-section for both setups, measured 120 mm downstream of the nozzle exit.**
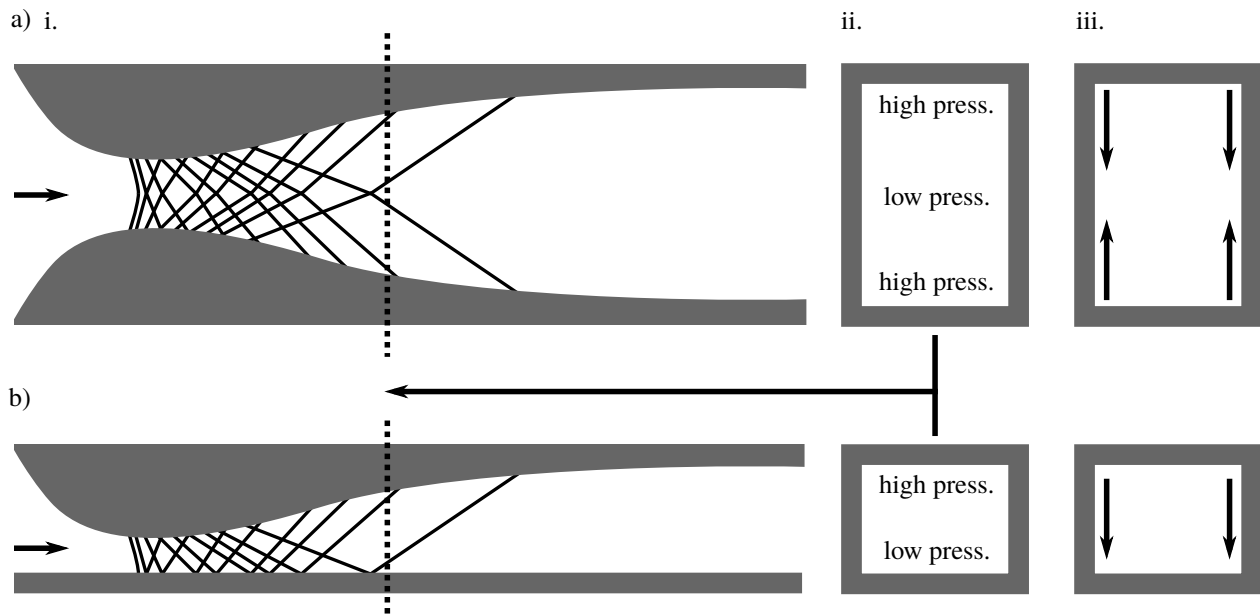
Fig. 3 Schematic of the hypothesised secondary flows for a) the full setup and b) the half configuration: i. inviscid expansion wave pattern through the nozzle; ii. the cross-sectional pressure distribution upstream of the nozzle exit; iii. induced secondary flows in sidewall boundary-layers.
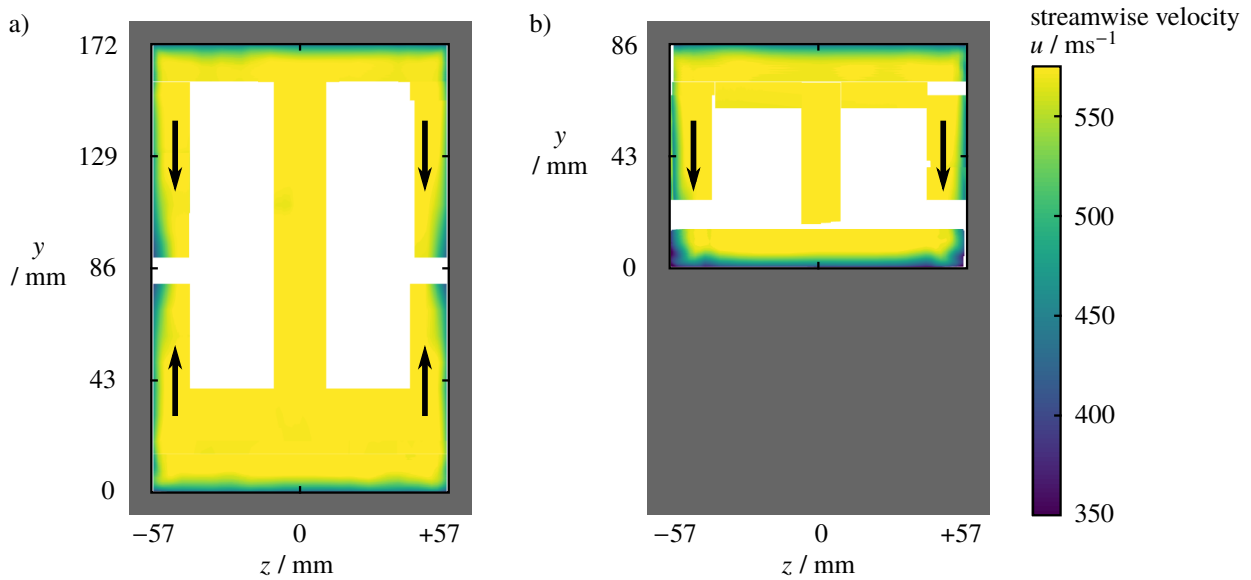

Fig. 4 The streamwise velocity (u) across the tunnel cross-section for both setups, measured 120 mm downstream of the nozzle exit. Direction of sidewall secondary flows are superimposed.
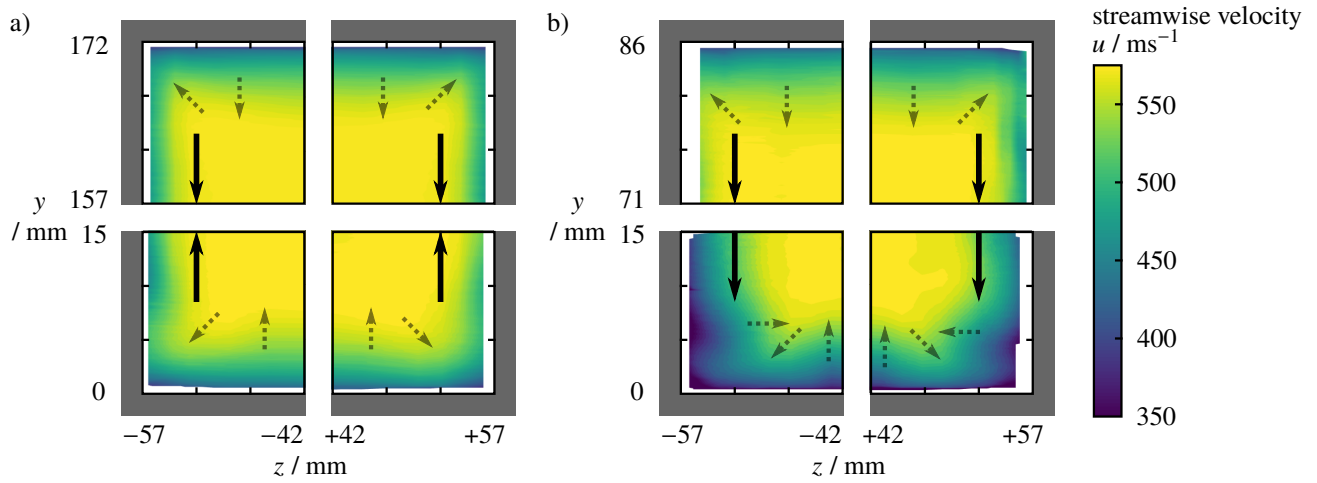
Fig. 5 The streamwise velocity (u) in 15×15 mm regions around all four tunnel corners for both nozzle setups. These are measured 120 mm downstream of the nozzle exit. Direction of sidewall secondary flows are identified by solid arrows. Indicative local regions of momentum transfer are shown by dashed arrows.
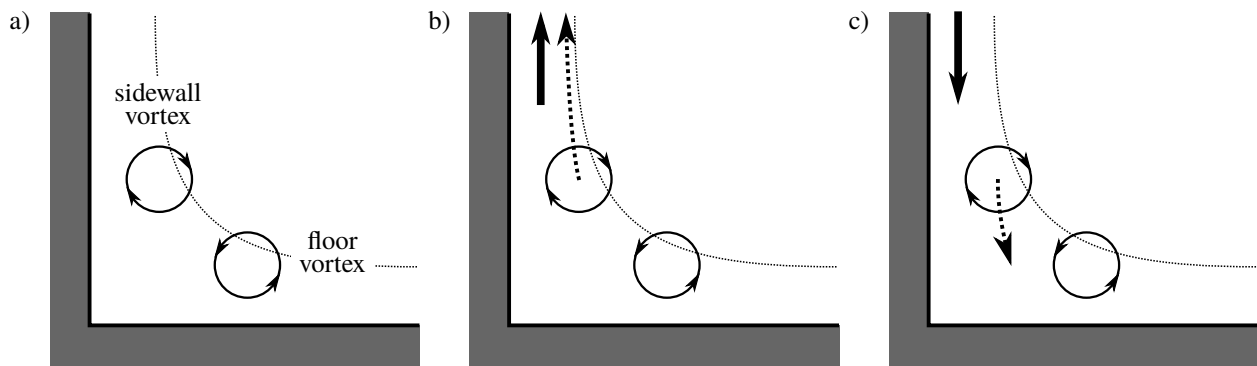

Fig. 6 Schematic diagram indicating the effect of sidewall secondary flows on corner vortex structure. The counter-rotating vortex pair with a) no vertical bulk flow, and the influence of vertical sidewall velocities b) away from and c) towards the corner are presented.